KINETIC MODEL OF NON METALLIC INCLUSIONS PRECIPITATION DURING STEEL SOLIDIFICATION.

Jean Lehmann, P. Rocabois, H. Gaye

IRSID - Voie Romaine - BP 320

F-57214 Maizières-lès-Metz Cedex France.

ABSTRACT.

A numerical simulation which describes precipitation of non metallic inclusions (liquid or solid oxides, nitrides) during steel solidification is proposed. Its aim is to predict the composition and size distribution of these precipitates. The model takes into account micro-segregation and includes homogeneous nucleation in the inter-dendritic liquid, and a mixed-controlled growth stage combining transport of solute elements in the boundary layer around precipitates and interfacial kinetics. It has been observed that the calculated compositions of oxide inclusions is different from that of inclusions precipitating at equilibrium and close to industrial observations on semi-killed steels.

1. INTRODUCTION.

Non metallic inclusions, such as oxides, sulphides or nitrides, formed during the solidification of steel, may change the metallurgical properties of various steel grades. Their morphology, size and distribution in steel are dominant factors, which affect some of the qualities, such as weldability, machinability or tensile strength in fatigue conditions. Therefore, a control of their size and spatial distribution is a means to improve the quality of some steel grades. IRSID has developed a model for predicting the nature, composition and total amount of inclusions, which precipitate in the metal during cooling and solidification under equilibrium conditions.

In order to obtain a better control not only on the nature, amount and composition of the inclusions but also of their size, morphology and spatial distribution, the mechanisms of their nucleation and growth have recently been studied by several authors[1,2,3,4]. A model has also been developed at IRSID in which nucleation, a mixed controlled growth mechanism and microsegregation are coupled[5,6] and the results delivered by this model have been compared to experimental results on TiN precipitation obtained by quenching during unidirectional solidification. In this paper, an extension of this model to the precipitation of multicomponent liquid oxides is presented.

2. THERMODYNAMIC BACKGROUND.

The thermodynamic analysis of the condition of oxide inclusions precipitation as a function of steel composition is based on IRSID's slag model[7,8] which provides reliable estimates of phase diagrams and component activities for the system:

SiO_2-TiO_2-Ti_2O_3-Cr_2O_3-Al_2O_3-Fe_2O_3-CrO-FeO-MnO-MgO-CaO-CaF_2-S.

This model has been integrated in the multiphase equilibrium calculation code CEQCSI[9] to compute equilibrium among the different phases involved in iron and steelmaking systems (liquid and solid metal, gaseous phases, slags, solid oxides, sulphides, nitrides, carbides,…). For calculation during solidification, an original method has been developed in which the

microsegregation equations for element dissolved in liquid metal, with diffusion in solid metal and equilibrium conditions between liquid steel and precipitates are solved simultaneously[10].

3. NUCLEATION AND GROWTH MODEL.

Nucleation.

The rate of homogeneous nucleation of inclusions given by the classical nucleation theory[11] is usually expressed as:

$$J^* = Z.\beta.N.\exp\left(-\frac{\Delta G^*}{kT}\right) \quad (1)$$

where Z is the Zeldovitch factor, β a frequency factor, N the number of nucleation sites per unit volume, ΔG^* the activation energy for the formation of critical nucleus, k Bolzmann's constant and T the absolute temperature.

For the nucleation of a pure component in its pure liquid, the number of nucleation sites by volume unit is taken equal to N_A/V where N_A is Avogadro's number and V is the molar volume of the liquid. It seems that this approach must be amended for nucleation in dilute solutions. For example, Kunze et al[12] proposed, for nucleation of TiN in a low alloyed steel, a correction factor equal to the product of the mole fractions of Ti and N. As a first attempt, and as most authors in this field, we have kept N_A/V_{Fe} (V_{Fe} is molar volume of liquid iron) for the nucleation site number but a more suitable approach for the nucleation of non-stoichiometric multicomponent precipitates in dilute solutions is necessary.

ΔG^* can be expressed in terms of interfacial energy (σ) and volume free energy change (ΔG_v):

$$\Delta G^* = (16\pi\sigma^3)/(3\Delta G_v^2) \quad (2)$$

The composition of the critical nuclei is assumed to be such that ΔG_v is minimum. Another expression of this condition is that the affinities of the reactions of formation of all oxide components of the oxide solution are equal. Their common value is the driving force of precipitation noted I whose expression is:

$$I = RT \ln\left(\frac{\left(a_{\underline{M}}\right)^x.\left(a_{\underline{O}}\right)^y}{K_{M_xO_y}.a_{M_xO_y}}\right)^{\frac{1}{x+y}} \quad (3)$$

where $K_{M_xO_y}$ is solubility product of M_xO_y in liquid metal, $a_{\underline{M}}$ and $a_{\underline{O}}$ are respectively the activities of element M and of oxygen referred to the 1% dilute solution and $a_{M_xO_y}$ is the activity of M_xO_y in the liquid oxides. If X_i represents the mole fraction of oxide i in the nuclei and C_{ji} the number of atoms j in the oxide i, ΔG_v is equal to:

$$\Delta G_v = I.\left(\sum_{i,j} C_{ji} X_i\right) / V_{oxide} \quad (4)$$

These quantities, oxide composition and driving force of precipitation, are directly obtained from the CEQCSI software.

The Zeldovitch factor Z is the number of oxide monomers, which can be added to or removed from the critical nuclei without modifying their energy by more than kT (Figure 1)[13]. It is given by

$$Z = \frac{1}{2\pi r_c^2} . \frac{V_{oxide}}{N_A} . \sqrt{\frac{\sigma}{kT}} \quad (5)$$

where V_{oxide} is the molar volume of liquid oxides and r_c is the radius of the critical nuclei:

$$r_c = -2\sigma / \Delta G_v \quad (6)$$

The proposed expression of the frequency factor β for non-stoichiometric compounds is (see Appendix):

$$\beta = 4\pi r_c^2 \sum_i \Gamma_i \quad (7)$$

where Γ_i represents the number of monomers of oxide i which are added per unit time and unit area to the nucleus.

Table I gives the expressions of Γ_i proposed by different authors[14-20]. Most of these expressions are function of the diffusion coefficients in liquid steel of the elements contained in the oxide or of the activation energies of these diffusion coefficients. When comparing the values delivered by the different models, they differ at most by a factor of 10^4 from around 10^{26} to 10^{30} nuclei.m^{-2}.s^{-1}. The expression given by LeGoues and Aaronson gives the smallest value and this value is compatible with a growth controlled by diffusion on an inclusion of critical radius as calculated for TiN[5,6] (Figure 2). For this reason, we have chosen the following expression, which is an extension to a stoichiometric compound containing several elements of the formalism proposed by these authors:

$$\Gamma_i = \frac{1}{a_0^4} \left(\prod_j \left(D_j . x_j \right)^{C_{ji}} \right)^{1/\sum_k C_{ki}} \quad (8)$$

where a_0 is the interatomic distance, D_j is the diffusion coefficient of the element j and x_j its atomic fraction in the metal

But, it has been shown for TiN[5] that the growth is limited by an interfacial kinetics and that, in this case, the flux on small precipitates is much smaller than in the case of a diffusion controlled growth (Figure 2). To take into account such phenomena, some authors[14,17,21] make the assumption of a diffusion through the interface metal/precipitate and consider an activation energy connected to an interfacial reaction instead of the activation energy of the volume diffusion coefficient. In the calculations presented in this paper, the Γ_i's have been modified to give flux values on critical nuclei compatible with an interfacial kinetics limitation.

Growth rate.

To describe the growth of a precipitate, it is assumed that a stationary diffusion state is reached and that each precipitate grows independently from the others. This hypothesis is verified as long as the mean distance between precipitates is much larger than their size, which is the case when the amount of precipitates is less than about 100 ppm. As for TiN[5], the

flux of atoms on the surface is described by a mixed controlled model in which the interfacial reaction is one of the limiting steps. The flux equations resulting from these assumptions are the following:

- the flux equations giving the flux of the different elements at the interface metal/inclusion. For element i, the expression of this flux is:

$$J_i = k_i.\left(C_i^{(m)} - C_i^{(i)}\right) \tag{9}$$

$C_i^{(m)}$ and $C_i^{(i)}$ are the concentrations in mol.m^{-3} respectively in the liquid steel far from the precipitate and the interfacial concentration (when the growth is diffusion controlled, $C_i^{(i)}$ is the equilibrium value). k_i is the transfer coefficient. In the case presented here, due to the small size of the precipitates, it is assumed to be equal to D_i/r where r is radius of the precipitate.

- the expression chosen for the flux due to the interfacial reaction involves only one kinetic constant k_c :

$$\dot{N} = k_c.\left(\exp\left(\frac{I^{(i)}}{RT}\right) - 1\right) \tag{10}$$

$\dot{N}$ is the flux of oxides (expressed in moles of oxide components per m^2 and per second), $I^{(i)}$ is the driving force of precipitation of the oxide phase from a metal which has the composition of the liquid steel at the interface. Due to the fact, as mentioned before, that this driving force is equal to the affinities of the reactions of formation of all oxide components, an expression of the flux can be expressed for each oxide. For example, for SiO_2, it would be:

$$J_{SiO_2} = \dot{N}.X_{SiO_2} = k_c.X_{SiO_2}.\left(\left(\frac{a_{\underline{Si}}^{(i)}.a_{\underline{O}}^{(i)2}}{K_{SiO_2}.a_{SiO_2}}\right)^{\frac{1}{3}} - 1\right) \tag{11}$$

where X_{SiO_2} is the mole fraction of SiO_2 in the appearing oxide phase, K_{SiO_2} is the solubility product and $a_{\underline{Si}}^{(i)}, a_{\underline{O}}^{(i)}$ are the silicon and oxygen activity at the interface referred to the 1% dilute solution.

The limitation due to interfacial kinetics is illustrated for TiN precipitates on Figure 3 which compares what would be the fluxes and the growth rates for a given supersaturation in the case of diffusion controlled growth and with an interfacial kinetics limitation[5] corresponding to two sulphur compositions. The kinetic constant has been assumed to vary with surface active elements, oxygen and sulphur, according to the formalism used for metal/gas reaction[22]. The difference between the fluxes in the diffusion-control and mixed-control models exceeds several orders of magnitude for submicronic precipitates, for which it is doubtful that very high fluxes consistent with a pure diffusional process could be accommodated at their interface.

4. APPLICATION OF THE MODEL.

The model has been applied to the precipitation of complex liquid oxides in a steel whose composition is given in Table II. The model uses the CEQCSI code to solve, for a succession

of small time intervals during metal solidification, the microsegregation equations[10], and to calculate the composition of the critical nuclei as well as the evolution of the composition of the existing precipitates. All the parameters used in the calculation are listed in Table III. Due to the lack of data, the kinetic constant chosen for this calculation has been supposed to be the same as the constant taken to reproduce the experimental data on TiN precipitation in a low-sulphur steel[5].

An example of the type of calculations performed at each moment is given on Figure 4. As Figure 3 for TiN, this figure gives the value of the flux on precipitates as a function of their radius. The order of magnitude of the diffusion flux for very small precipitates is much smaller than what has been calculated for TiN because of the much smaller concentrations of the diffusing elements in the case of oxide precipitation.

For liquid oxides precipitation, the determination of the flux requires the computation of composition of the new oxide layer which precipitates on existing inclusions (Figure 5). In particular, the partition Ti^{3+}/Ti^{4+} has be computed to fulfil the condition of equilibrium with the metal:

$$2Ti_2O_3 \rightarrow 3TiO_2 + \underline{Ti}$$

For very small precipitates, whose growth is controlled by interfacial kinetics, this composition does not depend on the radius and corresponds to the composition minimising the volume free energy change for the metal composition at the interface. For large precipitates whose growth is controlled by diffusion, the composition corresponds to the equilibrium composition with the metal at the interface. Since, for our application, we have chosen a mass transfer coefficient with a particular expression proportional to 1/r, it can be shown that this composition does not vary either with the precipitate radius. In the general case of the precipitates with intermediate sizes, whose growth is mixed controlled, the composition of the oxide layer depends on the radius.

Figure 6 compares the evolution with temperature of the amount of precipitated oxides calculated at equilibrium and with the kinetic model. At equilibrium, the precipitation starts already in the liquid steel whereas, in mixed controlled growth, even though the precipitation starts at the beginning of solidification, the amount of inclusions becomes noticeable only below 1492°C when the fraction of liquid metal phase is less than 7%. At this stage, at equilibrium, more than 95% of the total oxygen would already have precipitated.

At the end of solidification, in the kinetic model, the amount of precipitates increases sharply. However, at that stage, the amount of oxygen dissolved in ferrite (2 ppm, cf. Figure 6) is still larger that what would be predicted by an equilibrium calculation (0.5 ppm). This residual oxygen will precipitate in the solid metal probably as very small inclusions.

The late and sharp increase of the amount of precipitates observed in the kinetic model is the consequence of the competition between nucleation and growth to consume the supersaturation. Figure 7 which gives the evolution of the supersaturation with temperature and Figure 8 which gives the nucleation rate, show that, as long as the supersaturation is smaller than a critical value (about 7.5 in our example), the nucleation rate and, as a consequence, the amount of inclusions remain low. Then, when the supersaturation exceeds that critical value, the nucleation rate increases very rapidly and the amount of precipitated oxygen increases because of these new precipitates and of the growth of the existing ones. As long as the supersaturation is higher than the critical value, nucleation remains very effective and the most numerous inclusions are always the smallest ones as shown by the size histogram given on Figure 9 for a temperature of 1492°C.

Once the supersaturation starts decreasing, the nucleation rate falls, and then, when it becomes smaller than the critical value, the number of existing inclusions is much larger than the number of new ones. At this stage, the increase of the amount of precipitated oxygen is mainly due to the growth. The smallest inclusions which appear after the supersaturation maximum are less and less numerous as shown by Figure 9 for 1491°C. Thereafter the size histogram keeps the same shape, the sizes are just moving to the larger radii as shown by the size histogram at the end of solidification at 1484°C.

Thus, in the mixed-control mode, the time span during which precipitation occurs is quite limited. As a consequence, some trace element in the metal do not have enough time to be transported to the inclusions and their content in the precipitates are much lower than expected from equilibrium. Table IV shows that this is the case of Al for the example considered here and the average Al_2O_3 content of the inclusions at the end of solidification is far less than the content computed at equilibrium. Table V compares the compositions of oxide inclusions measured at the end of steel solidification for 3 industrial casts whose compositions are quite different from the composition considered above, to calculations performed at equilibrium. The equilibrium calculations overestimate the Al_2O_3 content and calculations at lower temperatures show that the differences would be even larger if we assume a re-equilibration in the solidified steel. So, it seems that a better agreement with the observations would be obtained by taking into account such a kinetic model.

5. DISCUSSION.

The calculation presented in this paper lies on several important simplifications, the most important ones being the assumption of an homogeneous interdendritic liquid, of a total rejection of the inclusions by the solidification front and the assumption of non-interacting particles. Due to the microsegregation, a concentration gradient exists in the interdendritic liquid near the solidification front and nucleation will preferentially take place in this zone as it is very sensitive to metal supersaturation. It is therefore certain that precipitation will start earlier than in the present calculation, and will very likely cover a wider temperature span, as the liquid interdendritic core will react more progressively with the nuclei. This emphasises also the importance of a realistic description of precipitates entrapment or rejection by the solidification front. Recent experimental and theoretical works[23,24] bring some helpful information in this domain. Ode et al. show[24], in particular, that the critical velocity of the solidification front which defines the transition between inclusion repulsion and engulfment, is mainly a function of the size of the particles: for a given cooling rate, the probability of an inclusion to be trapped by the solidification front increases with its size. Such a fact will have an important impact on the inclusions size and spatial distribution and further developments of the model will have to take into account these phenomena.

6. CONCLUSION.

The present study is an extension of the nucleation and growth model developed for the precipitation of stoichiometric compounds during metal solidification to the precipitation of multicomponent liquid oxides. The interfacial kinetic limitation has also been introduced in the description of inclusion growth with one single constant whose value, because of the lack of experimental data on liquid oxides, has been assumed to be equal to the one determined for TiN[5]. The expression of the nucleation rate has been modified to give flux values on critical nuclei compatible with this interfacial limitation.

Unfortunately, very few experimental results on size distribution are available in the domain of oxide inclusion precipitation during steel solidification, for comparison with model calculations. However, comparison with results of industrial casts on inclusions composition presented in this paper shows that the development of such a kinetic model seems to be necessary to obtain more accurate results than equilibrium calculations.

7. ACKNOWLEDGEMENTS.

The authors thank M. Kandel and J. Plagnieux for their helpful contributions.

8. LIST OF SYMBOLS.

a_0: interatomic distance (m)

a_j: activity of element j referred to the 1% dilute solution

$a_j^{(i)}$: activity of element j at the interface metal/precipitate referred to the 1% dilute solution

$a_{M_xO_y}$: activity of M_xO_y in the liquid oxides

h: Planck's constant ($6.6262.10^{-34}$J.s)

k: Bolzmann's constant ($1.38062.10^{-23}$J.K^{-1})

k_c: kinetic constant for the interfacial reaction (mol.m^{-2}.s^{-1})

k_j : mass transfer coefficient of element j in liquid steel (m.s^{-1})

n_S^* : number of atoms on the surface of a critical nucleus

r_c: radius of the critical nucleus (m)

x_i: mole fraction of element i in liquid steel

$C_i^{(i)}$: concentration of element i in the liquid steel at the interface metal/precipitate (mol.m^{-3})

C_{ji}: number of atoms j in a oxide molecule i

$C_i^{(m)}$: concentration of element i in the liquid steel far from the precipitate (mol.m^{-3})

D_j: diffusion coefficient of the element j in liquid steel (m^2.s^{-1})

$H(x_i)$: harmonic mean of x_i

I: driving force of precipitation of the oxide phase from a metal (J.mol^{-1})

$I^{(i)}$: driving force of precipitation of the oxide phase from a metal having composition of the liquid steel at the interface metal/precipitate (J.mol^{-1})

J*: nucleation rate (nuclei.m^{-3}.s^{-1})

J_i: flux of element i (mol.m^{-2}.s^{-1})

$J_{M_xO_y}$: flux of oxide M_xO_y (mol.m^{-2}.s^{-1})

$K_{M_xO_y}$: solubility product of M_xO_y in liquid metal

N: number of nucleation sites

N_A: Avogadro's number ($6.02217.10^{23}.mol^{-1}$)

Q_i: activation energy of diffusion ($J.mol^{-1}$)

R: gas constant ($8.3143\ J.K^{-1}.mol^{-1}$)

T: absolute temperature (K)

V_{Fe}: molar volume of liquid iron ($7.2.10^{-6}\ m^3.mol^{-1}$)

V_{oxide}: molar volume of liquid oxide ($m^3.mol^{-1}$)

X_i: mole fraction of oxide i in liquid oxide

Z: Zeldovitch factor

β: frequency factor (s^{-1})

η: metal viscosity ($m^{-1}.kg.s^{-1}$)

σ: interfacial energy between liquid metal and liquid oxides ($J.m^{-2}$)

ΔG^*: activation energy for the formation of a critical nucleus ($J.mol^{-1}$)

$\Delta G'$: activation energy of diffusion through the interface matrix/precipitate (J)

ΔG_v: volume free energy change associated to the formation of a nucleus from the liquid metal ($J.m^{-3}$)

Γ_i: number of monomers of oxide i added per unit time and unit area to the nucleus ($monomers.m^{-2}.s^{-1}$)

9. REFERENCES.

1. H. Goto, K. Miyazawa, K. Tanaka, "Effect of oxygen content on size distribution of oxides steels", ISIJ Int. 35(3), 1995, pp 286-291.

2. H. Goto, K. Miyazawa, W. Yamada, K. Tanaka, "Effect of cooling rate on composition of oxides precipitated during solidification of steel", ISIJ Int. 35(6), 1995, pp 708-714.

3. Z. Ma, D. Janke, "Characteristics of oxide precipitaion and growth during solidification of deoxidized steel", ISIJ int. 38(1), 1998, 46-52.

4. S. S. Babu, S. A. David, J. M. Vitek, K. Mundra, T. DebRoy, "Development of macro- and microstructures of carbon-manganese low alloy steel welds : inclusion formation", Materials Science and Technology, 11(2), 1995, pp 186-199.

5. H. Gaye, P. Rocabois, J. Lehmann, M. Bobadilla, "Kinetics of inclusion precipitation during steel solidification", Steel Research, 70, 1999, pp. 356-361.

6. P. Rocabois, J. Lehmann, H. Gaye, M. Wintz. "Kinetics of precipitation of non-metallic inclusions during solidification of steel". Journal of Crystal Growth, 198/199, 1999, pp. 834-843.

7. H. Gaye, J. Lehmann, "Modelling of Slag Thermodynamic Properties. From Oxides to Oxisulphides", Proc. 5th Int. Conf. on Molten Slags, Fluxes and Salts, ISS, 1997, pp. 612-617.

8. J. Lehmann, H. Gaye, "Thermodynamics Modeling of TiO_x Bearing Slags", Proc. 82nd Steelmaking Conference, Chicago, 1999, pp. 463-470.

9. C. Gatellier, H. Gaye, J. Lehmann, Y. Zbaczyniak, "Des outils thermodynamiques pour la maîtrise des réactions métal-laitier et le contrôle inclusionnaire des aciers", La revue de Métallurgie-CIT, 10, 1992, pp. 887.

10. M. Wintz, M. Bobadilla, J. Lehmann, H. Gaye, "Experimental study and modeling of the precipitation of non-metallic inclusions during solidification of steel", ISIJ Int. 35(6), 1995, pp. 715-722.

11. H. I. Aaronson, J. K. Lee, Precipitation processes in solids, ed. K.C. Russel et H. I. Aaronson, Conference Proceeding of the Metallurgical Society of AIME, Warrendale, PA, 1978, p. 31.

12. J. Kunze, C. Mickel, M. Leonhardt, S. Oswald, "Precipitation of titanium nitride in low-alloyed steel during solidification", Steel Research, 68, 1997, pp. 403-408.

13. J.B. Zeldovitch, Acta Physicochim., 18, 1943, p. 17.

14. J.W. Christian, The theory of transformation in metals and alloys, part 1, 2nd ed, Pergamon Press, Oxford, 1975.

15. F.K. LeGoues, H. I. Aaronson, "Influence of crystallography upon critical nucleus shapes and kinetics of homogeneous FCC-FCC nucleation – IV. Comparisons between theory and experiment in Cu-Co alloys", Acta Metall. 32(10), 1984, pp. 1855-1864.

16. E. A. Wilson, Worked examples in the kinetics and thermodynamics of phase transformation, The Institution of Metallurgists, London, 1981, 173 p.

17. D. Turnbull, J. C. Fisher, "Rate of nucleation in condensed systems" J. Chem. Phys. 17, 1949, pp. 71-73.

18. D. R. Uhlmann, H. Yinnon, "Glass Science and Technology, volume 1 glass forming system", ed. D.R. Uhlmmann and N.J. Kreidl, Academic Press inc., 1983, p 8.

19. G. H. Beall, D. A. Duke, "Glass Science and Technology, volume 1 glass forming system", ed. D.R. Uhlmann and N.J. Kreidl, Academic Press inc., 1983, p 406.

20. W. A. Tiller, "The science of crystallisation – Microscopic interfacial phenomena", University of Cambridge, pp. 339-377.

21. S. T. Dunham, I. Clejan, A. H. Gencer, Accurate and efficient modelling of nucleation and growth processes, Materials Science and engineering A238, 1997, pp. 152-159.

22. G.R. Belton, Metall. Trans. 24B, 1993, pp. 241-258.

23. H. Shibata, D.R. Poirier, T. Emi, "Modeling the behaviour of Al_2O_3 inclusions during the dendritic solidification of steel", ISIJ Int., 38(4), 1998, pp. 339-347.

24. M. Ode, J.S. Lee, S.G. Kim, Y. Suzuki, "Numerical Simulation of the Critical Velocity for Particle Pushing/Engulment Transition in Fe-C alloys using a phase-field model", ISIJ Int., 40(2), 2000, pp. 153-160.

Appendix: Expression of the nucleation rate for multicomponent oxide precipitates.

The steady state nucleation rate is calculated by assuming that nuclei grow by addition of single oxide monomer or shrink by elimination of single oxide monomer[11]. The flux of the nuclei containing p_1 molecules of oxide i, p_2 molecules of oxide 2,…,p_m molecules of oxide m (called (p_1,…,p_m) nuclei hereafter) is:

$$J_{p_1,..,p_m} = \sum_i \left(\beta^i_{p_1,..,p_m} N'_{p_1,..,p_m} - \alpha^i_{p_1,..,p_i+1,..,p_m} N'_{p_1,..,p_i+1,..,p_m} \right) \quad \text{(A1)}$$

where $\beta^i_{p_1,..,p_m}$ is the flux of monomers of oxide component i on a (p_1,…,p_m) nucleus, $\alpha^i_{p_1,..,p_i+1,..,p_m}$ is the frequency evaporation of monomers of oxide component i from a (p_1,…, p_i+1,…,p_m) nucleus, $N'_{p_1,..,p_m}$ is the actual number of (p_1,…,p_m) nuclei. Setting $N'_{p_1,..,p_m} = k_{p_1,..,p_m}.N_{p_1,..,p_m}$ where $N_{p_1,..,p_m}$ is the equilibrium number of (p_1,…,p_m) nuclei and using the relations (A1) and the fact that the flux is zero for the equilibrium distribution, we obtain:

$$J_{p_1,..,p_m} = -\sum_i \left(\alpha^i_{p_1,..,p_i+1,..,p_m} N_{p_1,..,p_i+1,..,p_m} \right) \frac{\partial k_{p_1,..,p_m}}{\partial p_i} \quad \text{(A2)}$$

The solution of this partial derivatives equation verifies the following system of equations:

$$\frac{\partial p_i}{\partial k_{p_1,..,p_m}} = -\frac{\alpha^i_{p_1,..,p_i+1,..,p_m} N_{p_1,..,p_i+1,..,p_m}}{J_{p_1,..,p_m}} \quad \text{(A3)}$$

After a summation on i and using the nullity of the flux for the equilibrium distribution, we obtain:

$$\frac{\partial p}{\partial k_{p_1,..,p_m}} = -\frac{N_{p_1,...,p_m}}{J_{p_1,..,p_m}} \sum_i \beta^i_{p_1,...,p_m} \quad \text{or} \quad \frac{J_{p_1,..,p_m}}{N_{p_1,...,p_m} \sum_i \beta^i_{p_1,...,p_m}} dp = -dk_{p_1,..,p_m} \quad \text{(A4)}$$

This equation is similar to the one obtained for the nucleation in a pure liquid. To calculate the flux from this equation, the following assumptions are usually made:

- the flux does not depend on the size of the nuclei but only on their composition i.e. $J_{p_1,..,p_m} = J_{X_1,..,X_m}$

- the number of (p_1,…,p_m) nuclei is zero (i.e. $k_{p_1,..,p_m} = 0$) if their size exceeds the critical size p* by a quantity 1/Z and is equal to the equilibrium number (i.e. $k_{p_1,..,p_m} = 1$) if their size is less than p*-1/Z.

Under these assumptions, the flux of nuclei is equal to:

$$J_{X_1,...,X_m} = 1 \Big/ \int_{p^*-1/Z}^{p^*+1/Z} \frac{dp}{N_{p_1,...,p_m} \sum_i \beta^i_{p_1,...,p_m}} \quad \text{(A5)}$$

Assuming that $\beta^i_{p_1,...,p_m}$ is proportional to the surface of the nuclei S_p and does not depend on their composition, we obtain:

$$J_{X_1,\ldots,X_m} = \sum_i \Gamma_i \Big/ \int_{p^*-1/Z}^{p^*+1/Z} \frac{dp}{S_p . N_{p_1,\ldots,p_m}} \qquad \text{(A6)}$$

If we take the same assumptions as usually taken for pure compound, that is S_p supposed to be practically equal to $4\pi r_c^2$ for p between p*-1/Z and p*+1/Z and the sum $\int_{p^*-1/Z}^{p^*+1/Z} \frac{dp}{N_{p_1,\ldots,p_m}}$ replaced by $1/\left(ZN^*_{p_1,\ldots,p_m}\right)$, we find:

$$J_{X_1,\ldots,X_m} = Z.\left(\sum_i \Gamma_i\right).N^*_{p_1,\ldots,p_m} \qquad \text{(A7)}$$

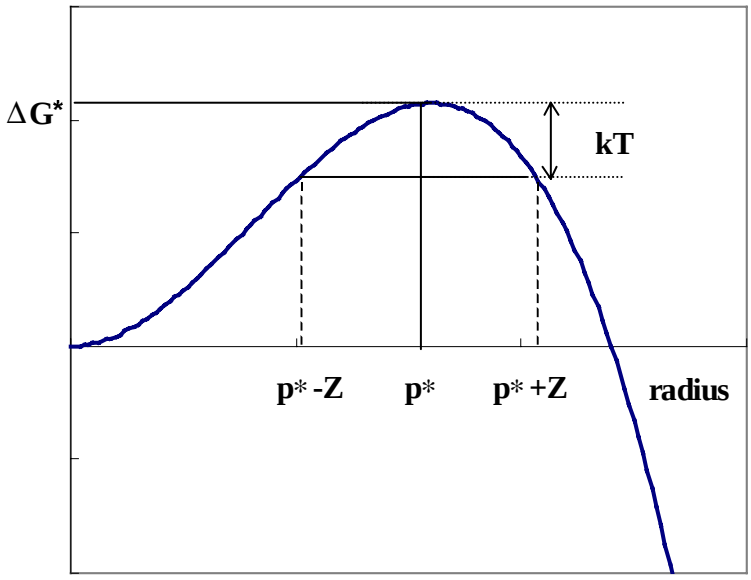

Figure 1: Definition of the Zeldovitch factor Z.

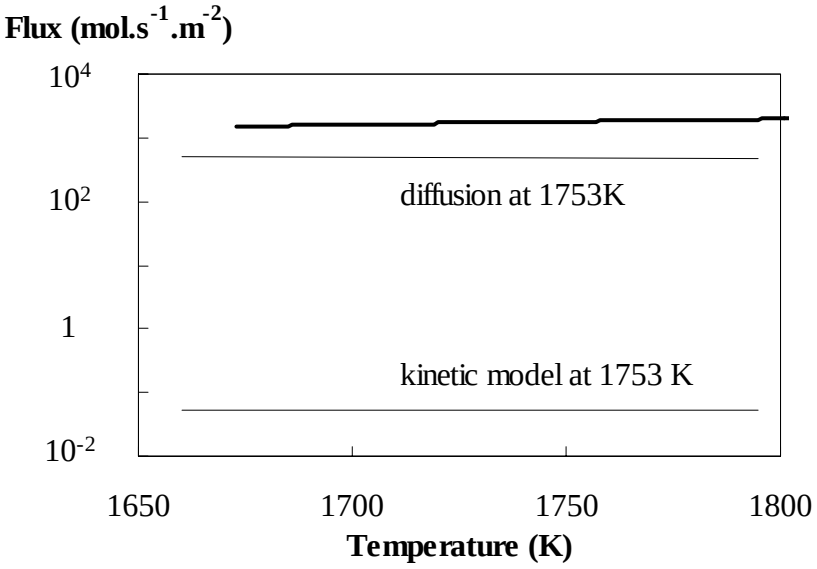

Figure 2: Flux (Γ/N_A) on critical nuclei of TiN given by LeGoues and Aaronson[15] model (heavy line) compared to calculated flux with diffusion and mixed-control growth model[5].

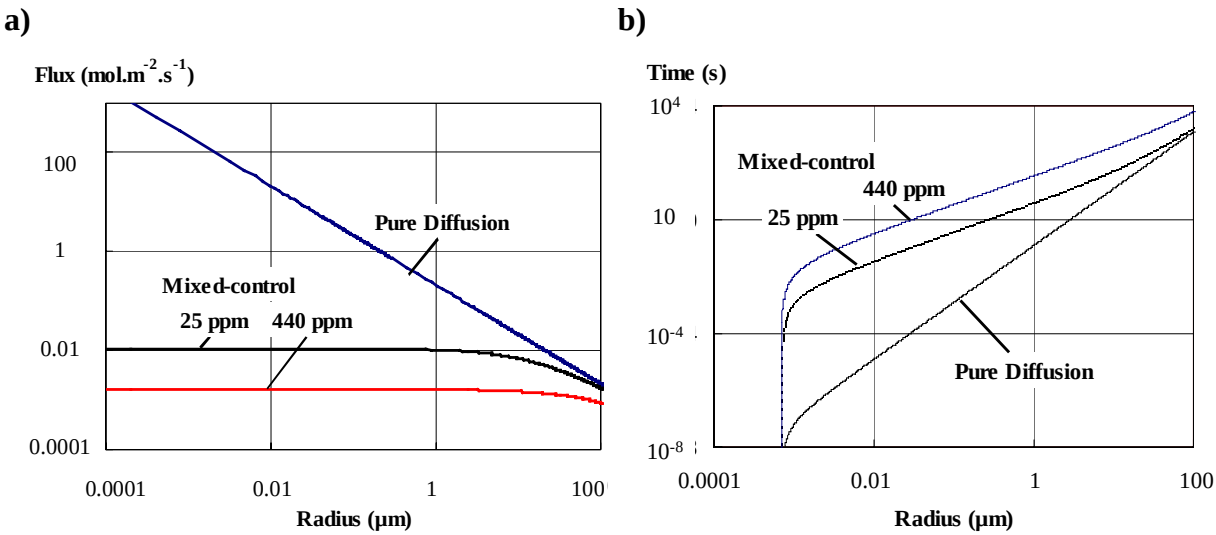

Figure 3: Comparison of the flux (a) and growth rate (b) in the diffusion-control and mixed-control models for TiN precipitates (constant degree of supersaturation $\exp(I/RT)=(a_{\underline{Ti}}.a_{\underline{N}}/K_{TiN})^{1/2}=2)^5$.

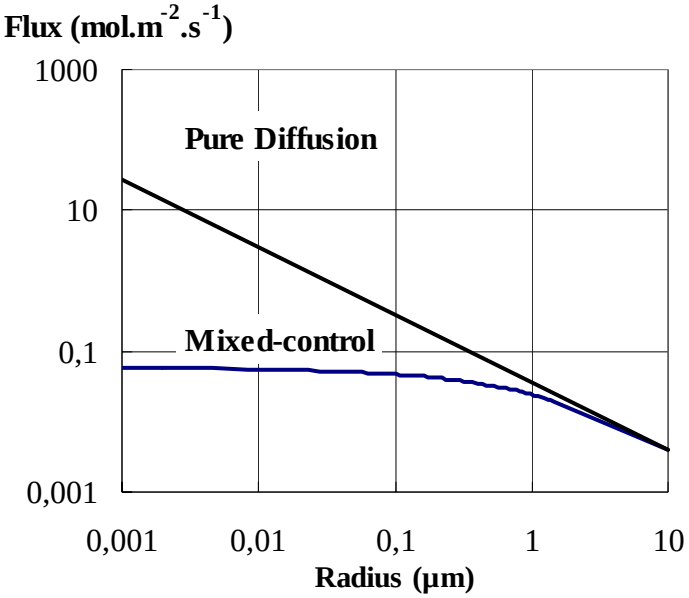

Figure 4: Comparison of the flux (sum of the moles of O, Al, Ti, Si and Mn) (a) and growth rate (b) in the diffusion-control and mixed-control models (supersaturation degree $\exp(I/RT)=6.7$).

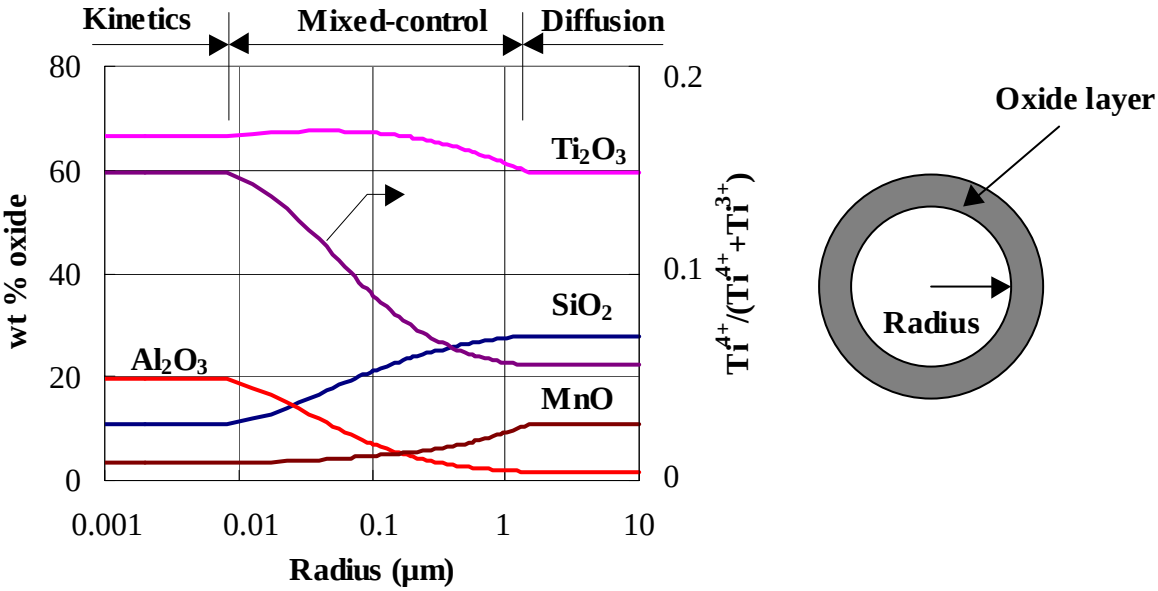

Figure 5: Composition of the new oxide layer precipitating on the existing precipitates as a function of their radius. The overall Ti-oxides content is expressed as wt % Ti_2O_3 but the proportion $Ti^{4+}/(Ti^{4+}+Ti^{3+})$ is also indicated.

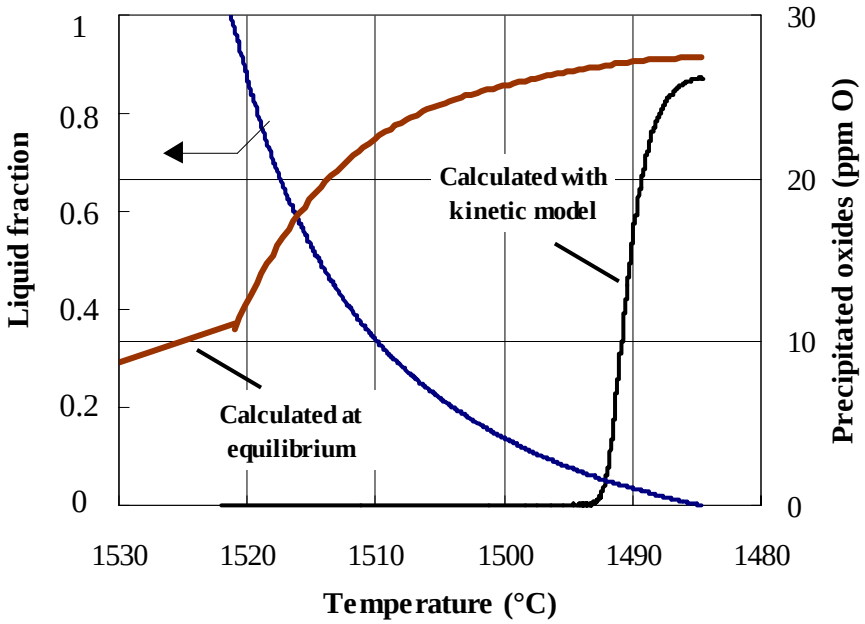

Figure 6: Calculated liquid fraction and amount of precipitated oxides at equilibrium and with mixed control growth model as a function of temperature.

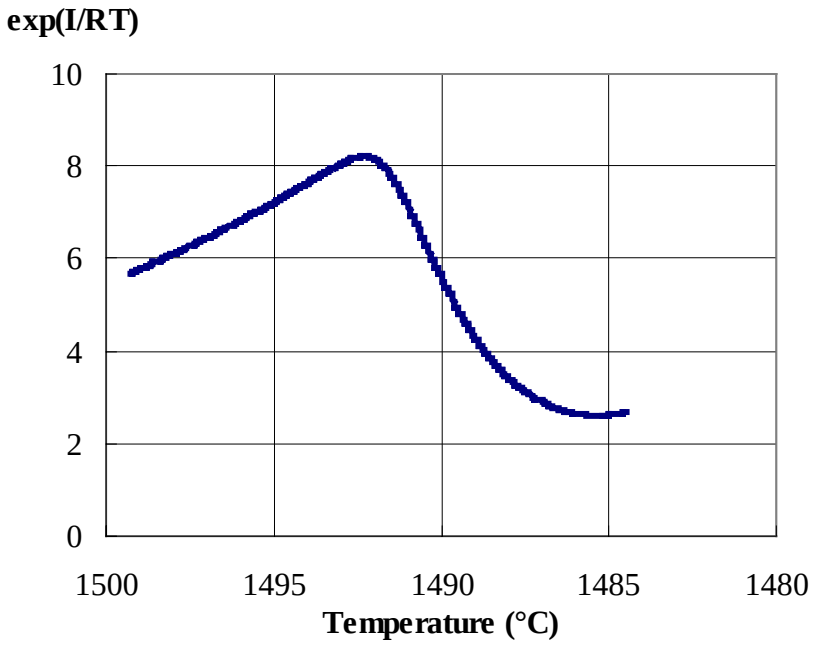

Figure 7: Evolution of the supersaturation with temperature during solidification.

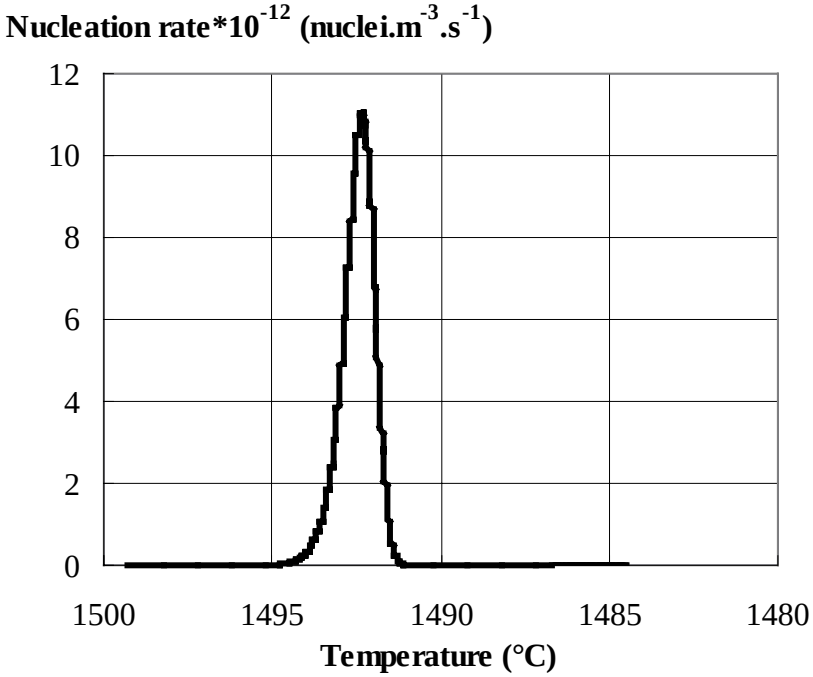

Figure 8: Nucleation rate as a function of the temperature.

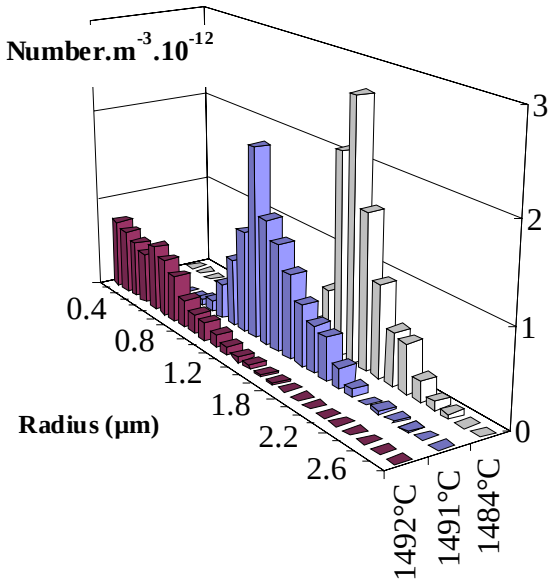

Figure 9: Evolution of the histogram of the inclusion sizes during the solidification.

Table I: Expression of Γ (cf. List of symbols). For clarity reason, with respect to the original papers, the notations have been unified.

Authors	Γ
Christian[14]	$\Gamma = n_S^* \frac{kT}{h} \exp(\frac{-\Delta G'}{kT}) / (4\pi r_c^2)$
Kunze et al.[Error! Bookmark not defined.]	$\Gamma = \frac{kT}{h} a_0 . H\left[x_i \exp(\frac{-Q_i}{kT}) \right]$
LeGoues and Aaronson[15]	$\Gamma_i = \frac{D_i x_i}{a_0^4}$
Wilson[16]	$\Gamma_i = \frac{D_i x_i^{(2/3)}}{a_0^2}$
Turnbull and Fisher[17]	$\Gamma = n_S^* \frac{kT}{h} \left(\frac{\sigma}{9\pi} \right)^{1/2} \exp(\frac{-\Delta G'}{kT}) / (4\pi r_c^2)$
Uhlmann[18]	$\Gamma = \frac{kT}{3\pi a_0^3} \frac{1}{\eta} / (4\pi r_c^2)$
Uhlmann[19]	$\Gamma = \frac{kT}{h} \exp(\frac{-Q}{kT}) / (4\pi r_c^2)$
Tiller[20]	$\Gamma = \frac{kT}{6ha_0^2} \exp(\frac{-Q}{kT})$

Table II: Steel composition (in wt %).

Al	C	Mn	Si	Ti	O
0.0010	0.085	1.370	0.155	0.011	0.0028

Table III: Calculation parameters.

Cooling rate	1.2 $K.s^{-1}$
Liquid/oxide interfacial energy	1.1 $J.m^{-2}$
Kinetic constant	0.01 $mol.m^{-2}.s^{-1}$
Al diffusion coefficient in liquid steel	3.10^{-9} $m^2.s^{-1}$
Mn diffusion coefficient in liquid steel	$4.9.10^{-9}$ $m^2.s^{-1}$
Si diffusion coefficient in liquid steel	$2.5.10^{-9}$ $m^2.s^{-1}$
Ti diffusion coefficient in liquid steel	$8.3.10^{-9}$ $m^2.s^{-1}$
O diffusion coefficient in liquid steel	$11.2.10^{-9}$ $m^2.s^{-1}$

Table IV: Average composition of the inclusions calculated at equilibrium and with the kinetic model.

	SiO_2	Ti_2O_3	Al_2O_3	MnO
Equilibrium	14	56	19	11
Kinetic model	28	60	2	10

Table V: Comparison of oxide inclusion compositions, at the end of steel solidification, analysed on industrial products and calculated at equilibrium.

	Sample #1		Sample #2		Sample #3	
	Calculated	Measured	Calculated	Measured	Calculated	Measured
Al_2O_3	37.5	23.8	29.9	12.2	48.8	24-42
SiO_2	7.8	2.4-4.7	7.7	1	2.8	1.8-3.2
TiO_x	42.1	56.2-63.4	53.1	67.7-69.8	35.2	40.5-63.8
MnO	3.7	2.3-6.8	7.5	14.3-17.4	1.6	1.3-1.4